ACS APPLIED MATERIALS & INTERFACES

Research Article

www.acsami.org

# Simultaneous Synthesis and Assembly of Silver Nanoparticles to Three-Demensional Superstructures for Sensitive Surface-Enhanced Raman Spectroscopy Detection

Yanqiong Yang,[†,‡] Wenqin Wang,*[,†,‡] Tao Chen,[§] and Zhong-Ren Chen*[,†,‡]

[†]Department of Polymer Science and Engineering, Faculty of Materials Science and Chemical Engineering, and [‡]Key Laboratory of Specialty Polymers, Grubbs Institute, Ningbo University, Ningbo 315211, P. R. China

[§]Division of Polymers and Composite Materials, Ningbo Institute of Materials Technology and Engineering, Chinese Academy of Science, Ningbo 315211, P. R. China

Supporting Information

**ABSTRACT:** Construction of superstructures with controllable morphologies from NPs is of great scientific and technological importance. A one-step method for simultaneous synthesis and assembly of Ag NPs to three-dimensional (3D) nanoporous superstructures is demonstrated. By varying the adsorption time of Ag precursors, an array of well-defined Ag superstructures with different morphologies are harvested. A "hot spot"-rich substrate for surface-enhanced Raman spectroscopy is established, which exhibits high sensitivity in trace detection of molecules. It is believed that the presented 3D nanoporous Ag superstructures hold great potential for various uses, such as novel multifunctional sensing and monitoring chips or devices.

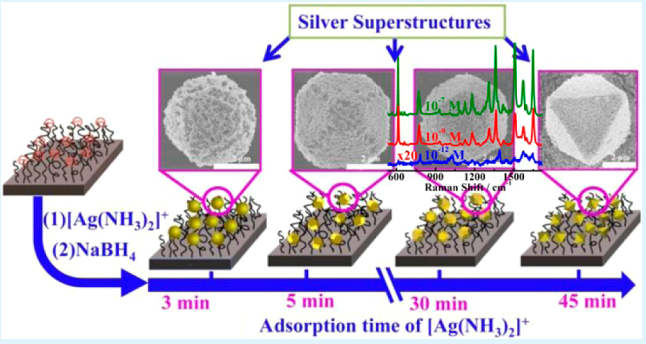


**KEYWORDS:** *superstructures, tunable morphology, self-assembly, three-dimension, polymer brushes, SERS*

## 1. INTROCUTION

Organizing nanoparticles (NPs) into hierarchical three-dimensional (3D) superstructures is a prevalent topic in science.[1−3] Architectually well-defined metal superstructures are vital to explore their remarkable collective properties and eventually to transform nanoscale science into applicable nanotechnology.[4−7] However, the achievement of metal superstructures and the controlling of their morphological diversity are still at an elementary level. First, as-prepared NPs with precise sizes and shapes, which dictate the overall superstructure design, are usually needed.[6,7] Second, most of the reported methods usually take two steps and need complex operating procedures or strict experimental conditions or precise control that seriously limit the quality, quantity, and reproducibility of such superstructures.[4,5,8] Furthermore, there are only a few methods for fabrication of 3D nanoporous superstructures, which is desirable for more applications in catalysis, optoelectronics like surface-enhanced Raman spectroscopy (SERS), sensing, etc.[9−11] It is therefore still a challenge to establish a simple, robust, and easily-operated self-assembly method to generate 3D nanoporous metal superstructures.

SERS in particular has drawn significant attention due to its capability to dramatically enhance the Raman signals. It has been intensively studied for decades as a promising strategy for potentially enabling the label-free detection of small biomolecules at low concentrations and even allows single-molecule level detections.[12−14] The key factor for ideal SERS substrates is the amount of electromagnetic "hot spots", a point with a strongly enhanced local field, which allows extremely sensitive SERS detection.[14]

Here, we report a one-pot approach for simultaneous synthesis and self-assembly of Ag NPs to micrometer-sized Ag superstructures in the presence of polymer brushes. The shapes of Ag superstructures can be tuned by adjusting the fabrication condition. The Ag superstructures consisted of heterogeneous NPs exhibit nanoporous and networking architectures with the size of about 50 nm in three-dimension. A novel 3D hot spot-rich SERS substrate is established based on the nanoporous superstructures. SERS shows that the prepared 3D nanoporous Ag superstructures exhibit high sensitivity in trace detection of molecules.

Polymer brushes, as the nanoscale assemblies of macromolecules by one end to substrates[15,16] with excellent physicochemical properties, are promising as the versatile and favorable substrate or matrices for generating NPs.[8,9,15,17−20] Here, we first report about synthesis and assembly of NPs to generate 3D nanoporous superstructures on polymer brushes in one step, as shown in Figure 1.

**Received:** September 19, 2014
**Accepted:** October 28, 2014
**Published:** October 28, 2014

  

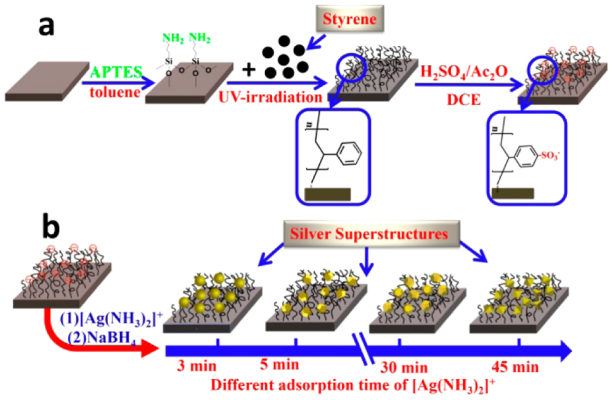


**Figure 1.** Schematic illustration of the procedures for synthesis and sulfonation of polymer brushes (a) and preparation of silver superstructures with controllable morphologies (b).

## 2. EXPERIMENTAL SECTION

**2.1. Materials.** Styrene (99%, Alfa Aesar) was purified by neutral $Al_2O_3$ column and dried with a 0.4 nm molecular sieve at room temperature. 3-Aminopropyltriethoxysilane (APTES, 98%, Alfa Aesar), $Al_2O_3$, $AgNO_3$ (99.8%), $NH_4OH$ (25%), $H_2O_2$, 1,2-dichloroethane, acetic anhydride (98.5%), concentrated sulfuric acid, anhydrous ethanol, ethyl acetate, and $NaBH_4$ were obtained from Sinopharm Chemical Reagent Co. (Shanghai, China). All were used as received without further purification.

N-doped, (100)-oriented silicon wafers solid substrates were used. Silicon wafers were cleaned in a mixture of $H_2O_2/H_2SO_4$ (1:3, v/v) at 80 °C ("piranha solution") for 2 h, washed thoroughly with Milli-Q-grade water, and dried in a stream of $N_2$ before APTES deposition. (*Caution: Piranha solution reacts violently with organic matter!*).

**2.2. Polymer Brush Synthesis.** Initially, homogeneous polymer brushes were prepared on flat silicate substrate. A freshly prepared OH-terminated silicon substrate, which was treated with fresh piranha solution, was immersed in a 5% APTES anhydrous toluene solution and sonicated for 30 min. Then, APTES molecules were attached as linker molecules via a silanization reaction. With the amino group pointing toward the outer interface, this structure offered activity sites for grafting polymer brushes by self-initiated photografting and photopolymerization (SIPGP) of styrene or other vinyl monomers. After thorough cleaned and dried by nitrogen, the APTES-functionalized silicon substrate was submerged in bulk styrene and irradiated for 1.5 h with an UV-light lamp with the spectral distribution between 300 and 400 nm ($\lambda_{max}$ = 350 nm) for the SIPGP. Then, sulfonation of polystyrene (PS) brushes after all phsiadsorbed polymer molecules were carefully removed by ultrasonic irradiation in several solvents of different polarities, dried in a jet of nitrogen. The method for sulfonating PS brushes accords to previous report.[21]

**2.3. Ag Superstructure Preparation.** Finally, as shown in the Scheme S1b, when the as-prepared poly(styrene sulfonic acid) (PSSA) brushes were immersed in the slightly alkaline Tollens reagent (1 mM, 10 mL) for different time, the positively charged $[Ag(NH_3)_2]^+$ was adsorbed to the negatively charged PSSA brushes via ion-exchange and electrostatic interaction. After rinsing with an amount of water to wash away unstable adsorption ions, the substrate was treated with a freshly prepared ice aqueous solution of $NaBH_4$ for 10 min to fabricate silver superstructures.

**2.4. Preparation of Samples for SERS Measurements.** SERS substrates were prepared by immersion of the different samples in R6G aqueous solution for 3 h. Afterward, the samples were cleaned repeatedly with ethanol to remove the nonadsorbed R6G molecules. Raman spectra were recorded after the evaporation of ethanol.

**2.5. Characterizations.** Atomic force microscopy (AFM) images were taken by a multimode AFM (Being Nano-Instruments, Ltd.) operating in the tapping mode using silicon cantilevers (spring constant: 3–40 N $m^{-1}$, resonant frequency: 75–300 kHz). In order to verify the formation of (3-aminopropyl)triethoxysilane (APTES) and polymer brushes layer, attenuated total reflectance infrared (ATR-IR) spectra were recorded. X-ray photoelectron spectroscopy (XPS) was performed using the AXIS ULTRA DLD spectroscope (Kratos Analytical Ltd., Manchester, UK).

The scanning electron microscopy (SEM) images, which were obtained by using the field emission scanning electron microscope (SU-70) equipped with an energy dispersive X-ray system, were used for determining the morphologies of the Ag superstructures. Transmission electron microscopy (TEM) was recorded by a transmission an electron microscope (JEM-2100F, accelerating voltage of 200 kV). TEM samples were prepared by dropping a diluted aqueous solution of superstructures onto carbon-coated copper grids and dried in air. X-ray diffraction (XRD) by carrying out on a Rigaku D/max-RA X-ray diffraction meter using Cu K$\alpha$ radiation ($\lambda$ = 1.5418 Å). UV–vis absorption spectra of the samples were recorded using a Lambda 950 spectrophotometer (PerkinElmer). Spectrum was recorded by drying the superstructures dispersion onto a quartz substrate. A clean quartz wafer was used as the background.

SERS spectra were measured with a confocal microscope (Renishaw in Via Reflex). A laser with a wavelength of 532 nm and a power of 120 $\mu$W was focused on sample surface with a spot size 1 $\mu$m in diameter and the Raman signal was collected during an integration time of 1 s.

## 3. RESULTS AND DISCUSSION

As illustrated in Figure 1, we first prepare PSSA brushes.[22,23] Then immersing the PSSA brushes in the $[Ag(NH_3)_2]^+$ solution for different time results in different adsorption amount of $[Ag(NH_3)_2]^+$ precursors on the PSSA brushes. The morphology controllable Ag superstructures are produced on polymer brushes after reduction of adsorbed precursors by $NaBH_4$ in one step, as shown in Figure 1b.

ATR-IR spectra are performed to confirm the successful synthesis of the organic layer on the substrate (Figure S1). The CH and NH stretching modes found in the ATR-IR spectrum confirm the successful synthesis of the organic layer on the substrate. Two dominant vibrational modes are found at around 1575 and 1485 $cm^{-1}$ in the spectrum of APTES, which were assigned to the amino groups.[24] Several characteristic stretching vibrational bands are observed in the spectrum of PS brushes, such as C–H at around $\nu$ = 3025 $cm^{-1}$ and C–C at $\nu$ = 1445, 1490, and 1599 $cm^{-1}$.[22,24] The successful silanization reaction of 3-aminopropyltriethoxysilane and polymerization of monomers, and the sulfonation of the PS brushes are also demonstrated by X-ray photoelectron (XPS) spectra (Figure S2). For the PSSA brushes, C 1s and O 1s peaks are visible at around 285.0 and 532.0 eV, respectively. The N 1s peak at 400.0 eV is attributed to $NH_2$ terminal groups of APTES layer. The S 2s and S 2p peaks centered at 229 and 164 eV, respectively, are assigned to the aromatic sulfonic acid group of PSSA. Additionally, AFM characterization is done to investigate the thickness of the PS brushes. In Figure S3, before the AFM characterization, the brushes surface is scratched with a metallic needle gently in order to locally remove PS brushes layer and leave the hard silicon substrate intact. The border of the scratch is imaged by AFM and analysis of the height difference between the intact and the scratched surface areas gives the thickness of the brush layer approximately 60 nm. As the trace is scratched very gently, the real thickness of the polymer brushes should be large than 60 nm and the AFM image also suggests that the polymer brushes is very uniform and dense without obvious defects.

The as-prepared polymer brushes here are considered as the excellent "reactors" for the synthesis and assembly of silver NPs. Figure 2a and b shows the SEM images of the sample

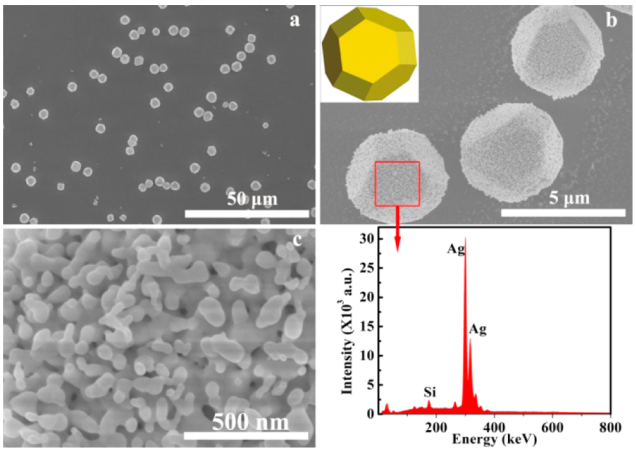


**Figure 2.** (a, b) SEM images of C30 at different magnifications. (b, inset) Typical model of ideal tetrakaidecahedral particle. (c) High resolution SEM image. (d) EDS of Ag superstructures, the area donated by the red square in part b.

C30. (C30 is referred to the sample fabricated on the polymer brushes with $[Ag(NH_3)_2]^+$ ions adsorption for 30 min, and reduction using $NaBH_4$ solution for 10 min). During the adsorption procedure, the $[Ag(NH_3)_2]^+$ precursors can be adsorbed in the matrix of polymer brishes. After reduction, extensive particles with the size of about 3−5 $\mu$m can be observed in Figure 2a at low magnification. Typical shaped surface is also seen clearly. At higher magnification in Figure 2b, the SEM image of three typical particles indicates that they are tetrakaidecahedron (the inset of Figure 2b) and exhibits obvious 3D feature. Fine details of tetrakaidecahedral Ag particles show that they consist of much smaller and heterogeneous NPs and exhibit nanoporous structures with a size of about 50 nm (Figure 2c), and this suggests that Ag superstructures with 3D complex structures and architecture are generated successfully through a route of simultaneous synthesis and assembly of Ag NPs. Nanoporous structures are clearly seen in the typical SEM image of one broken particles (Figure S4). Furthermore, the building blocks of Ag NPs are observed to be connected to each other, exhibiting networking architecture. The generation of Ag superstructures is also confirmed by the transmission electron microscopy image (Figure S5). The formation of Ag superstructures is further characterized by XRD (Figure 3a). The XRD pattern of Ag superstructures shows obvious peaks corresponding to the (111), (200), (220), and (311) diffraction peaks of fcc Ag, which confirms that Ag superstructures exist in crystalline state. To investigate the composition of the superstructures, the energy dispersive spectrum (EDS) (Figure 2d) and XPS spectrum is given (Figure S2). The obvious Ag peaks in the EDS and Ag XPS peaks at 374.2 ($Ag_3d_{3/2}$) and 368.2 eV ($Ag_3d_{5/2}$) in XPS evidence the presence of the Ag structures.[25] Furthermore, the difference between the doublets of Ag 3d electronic state of 6.0 eV suggests the presence of $Ag^0$ in the fabricated Ag superstructures, consistent with the XRD analysis.[25] A strong absorption peak at around 429 nm can be observed in the absorption spectrum, as displayed in Figure 3b, which is assigned to the surface plasmon resonance of Ag superstructures.

To further study the forming process of the Ag superstructures, we first exploit the impact of the time of $[Ag(NH_3)_2]^+$ adsorption on the resultant structures with the

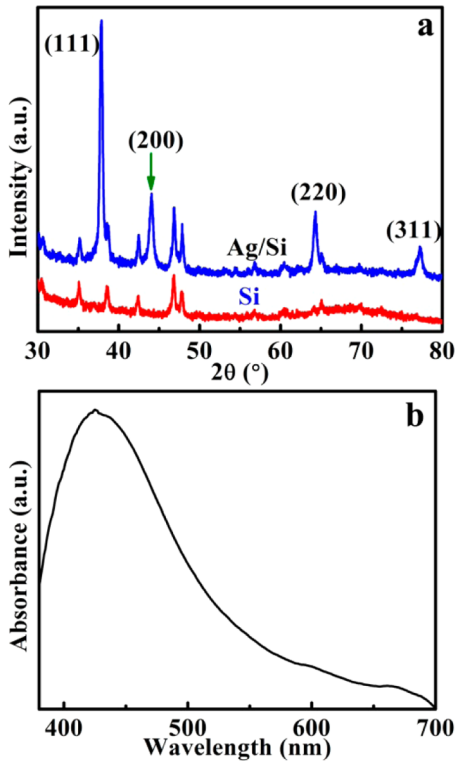


**Figure 3.** (a) XRD pattern of C30 and silicon and (b) absorption spectrum of C30.

time set to be 3, 5, and 45 min with the corresponding products named as C3, C5, and C45, respectively. The reduction time is about 10 min in all cases. Extensive micrometer-sized superstructures are also observed in Figure 4a, c, and e at low magnification. The typical high resolution SEM images of C3 (b), C5 (d), and C45 (f) in Figure 4 reveal that

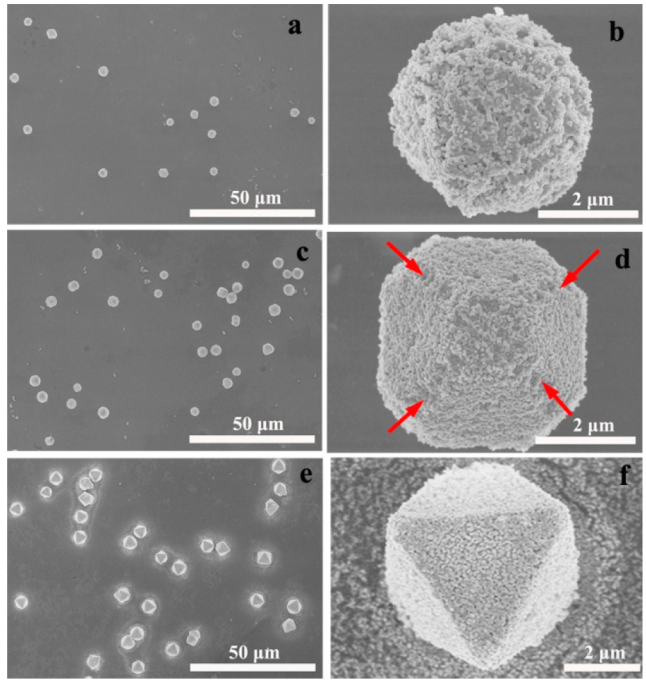


**Figure 4.** SEM images of Ag superstructures of (a, b) C3, (c, d) C5, and (e, f) C45.


dx.doi.org/10.1021/am506464f | ACS Appl. Mater. Interfaces 2014, 6, 21468−21473

superstructures possessing diverse geometric features with 3D heterogeneous architectures can be generated by adjusting the adsorption time of $[Ag(NH_3)_2]^+$. The Ag superstructures of C3 exhibit nearly spherical shape with nonuniformly rough surface (Figure 4b). For C5 (Figure 4d), 14 faces can be determined, which can be referred to be truncated octahedron with the typical corners of octahedron cut (namely corner-truncated octahedron). Additionally, the edges, pointed by the red arrows, are not intact, appearing like an etched zone and distributing symmetrically. Increasing the adsorption time to 30 min results in shape evolving to tetrakaidecahedron (Figure 2b). Furthermore, the morphology of Ag superstructures can be converted from tetrakaidecahedron (C30) to well-defined octahedron (C45, Figure 3f).

Switching the reducing agent $NaBH_4$ to glucose, superstructures are also generated (Figure S6). However, these superstructures are nearly spherical with significantly rough surfaces, and no featured geometric shapes are seen; Ag particles are closely packed together in the superstructures (inset of Figure S6). The size of the Ag particles consisting of the superstructures is much larger than that of C30. Therefore, these results indicate that the reducing agents influence the resultant morphologies. The different resultant morphologies may stem from the different reduction rate using different reducing agents. The reduction rate is much faster with $NaBH_4$ as the reducing agent than that with glucose and more Ag NPs could be produced simultaneously, which results in smaller Ag NPs constituting the superstructures. With glucose as the reducing agent, the reduction rate of Ag precursors is very slow and this leads to growth of Ag NPs, generating larger ones, which was confirmed by the SEM images (Figure S6). As a result, the Ag NPs are too large to form superstructures with well-defined surfaces.

There are intensive investigations about fabrication of superstructures through the assembly of NPs, originating from a variety of interparticle interactions including van der Waals (vdW) force, dipole−dipole interactions, electrostatic forces, entropic effects, and other interactions.[1,26,27] However, unlike most previous reports, in which presynthesized NPs were adopted for the assembly, the synthesis and assembly of Ag NPs are simultaneous here. Furthermore, the Ag superstructures show nanoporous and networking architectures. Herein, when the substrate containing $[Ag(NH_3)_2]^+$ is immersed into the $NaBH_4$ solution, numbers of small Ag NPs can be produced in short time. These Ag NPs may assemble into superstructures with controllable morphologies through "oriented attachment", which can be assisted by the interaction of Ag NPs and organic molecules constituting of the polymer brushes via electrostatic assembly and under energy gain, thus creating extended 3D nanoporous superstructures (Figure 2c).[9,28−34] Furthermore, increase of adsorption time will increase the amount of adsorbed $[Ag(NH_3)_2]^+$ and subsequently increase the Ag NPs.[35] The appropriate ratio of $[Ag(NH_3)_2]^+$ or NPs to organic molecules is suggested to control the morphology, which may be determined by an energy-stabilization process.[10,11] In addition, using the glucose as the reducing agent, the formed Ag NPs may be too large to be arranged into a well-defined superstructures with oriented attachment and/or electrostatic assembly. More work about the production mechanism of Ag superstructures is in progress.

As displayed in Figure 2, the 3D nanoporous and networking superstructures contain many nanogap and connected nanoscale channels. The nanogap-rich Ag superstructures can generate strongly localized and high-density hot spots on the whole superstructures to increase SERS enhancement factor.[11,14,36,37] To test the Raman enhancing capability, an aqueous solution of Rhodamine 6G (R6G) with different concentration is applied to the 3D SERS substrates (C30), and Raman spectra are recorded. As shown in Figure 5a, the

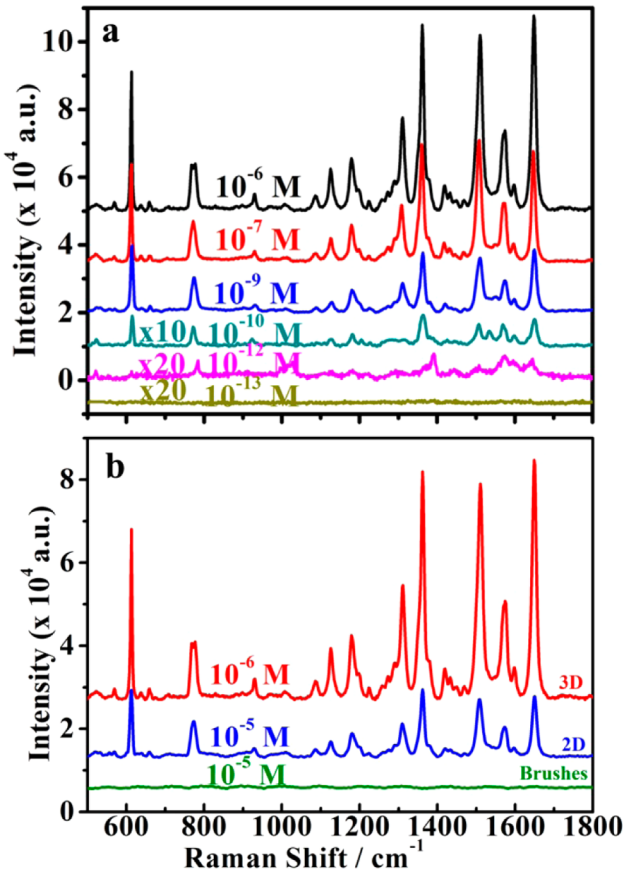


**Figure 5.** (a) Raman spectra with different concentrations of R6G adsorbed on superstructures. (b) Raman spectra of $10^{-6}$ M R6G on 3D superstructure-based substrates and $10^{-5}$ M on 2D Ag nanoparticle and polymer brushes substrates.

characteristic peaks at 613, 772, 1182, 1362, 1510, 1574, and 1650 $cm^{-1}$ assigned to R6G are generally in agreement with those reported previously.[38] When the concentration of R6G is even as low as $10^{-12}$ M, obviously enhanced Raman peaks can be observed, and a curve of concentration dependent SERS intensity (1510 $cm^{-1}$) is also provided in Figure S7.[39,40] We also compare the Raman-enhancing capability of 3D superstructure to that of Ag NPs by deposition Ag NPs on the PSSA brushes surface (namely "2D", as shown in Figure S8) and that of pure polymer brushes. Figure 5b indicates that the 3D SERS substrate ($10^{-6}$ M R6G) provides much higher SERS signal than 2D Ag substrate ($10^{-5}$ M R6G). No visible Raman peaks of R6G can be observed on the pure polymer brushes. These results indicate that 3D superstructures are an effective SERS substrate. The ultrahighly sensitive detection ability and the SERS intensity difference between 3D SERS substrate with 2D SERS substrate mainly results from high density hot spots of the 3D superstructures.[36,37] The performance of a SERS substrate is determined by two major factors, i.e., the enhancement factor and the number of probed molecules within a detection volume.[14,41,42] High density hot spots from

Ag 3D superstructures increase the areal density of hot spots within a detection volume. Thus, SERS enhancement factor and the number of probed molecules within a detection volume are increased. In addition, compared to 2D SERS substrate, 3D nanoporous structures provide a large specific surface area to interact with analytes, and the ease for the analytes to access the surfaces of AgNPs.[14,42]

## 4. CONCLUSION

In conclusion, we have developed a novel route to 3D Ag superstructures with controllable morphologies on polymer brushes. The synthesis and assembly of Ag NPs are achieved simultaneously. Remarkably, the superstructures exhibit complex 3D nanoporous and networking features. We propose that the simultaneous synthesis and assembly process results from the oriented attachment of Ag NPs, facilitated by a layer of polymer brushes. The assembly procedures described here may thus give access to a wide range of metal superstructures with tunable morphologies. 3D nanoporous Ag superstructures hold high promise for extensive applications, such as 3D trace detection, sensors, and photocatalysis.

## ■ ASSOCIATED CONTENT

### Ⓢ Supporting Information

Experimental procedures and characterization details. This material is available free of charge via the Internet at http://pubs.acs.org.

## ■ AUTHOR INFORMATION

### Corresponding Authors

*E-mail: wqwang@126.com (W.W.).
*E-mail: chenzhongren@nbu.edu.cn (Z.-R.C.).

### Author Contributions

All authors have given approval to the final version of the manuscript.

### Notes

The authors declare no competing financial interest.

## ■ ACKNOWLEDGMENTS

This work was sponsored by K. C. Wong Magna Fund in Ningbo University, National Science Foundation of China (NSFC 21274070), Key Team of Scientific Innovation of Zhejiang Province (No.2011R50001), and Ningbo "3315" Plan (No. 2012S0001). Ningbo S&T Program for Biomimetic Materials (No. 2011A31002), Excellent Youth Foundation of Zhejiang Province (LR14B040001).

## ■ REFERENCES

(1) Nie, Z. H.; Petukhova, A.; Kumacheva, E. Properties and Emerging Applications of Self-assembled Structures Made from Inorganic Nanoparticles. *Nat. Nanotechnol.* **2010**, *5*, 15−25.
(2) Rycenga, M.; Cobley, C. M.; Zeng, J.; Li, W.; Moran, C. H.; Zhang, Q.; Qin, D.; Xia, Y. Controlling the Synthesis and Assembly of Silver Nanostructures for Plasmonic Applications. *Chem. Rev.* **2011**, *111*, 3669−3712.
(3) Li, L.; Wang, Q. Spontaneous Self-Assembly of Silver Nanoparticles into Lamellar Structured Silver Nanoleaves. *ACS Nano* **2013**, *7*, 3053−3060.
(4) Wang, T.; Zhuang, J.; Lynch, J.; Chen, O.; Wang, Z.; Wang, X.; LaMontagne, D.; Wu, H.; Wang, Z.; Cao, Y. C. Self-Assembled Colloidal Superparticles from Nanorods. *Science* **2012**, *338*, 358−363.
(5) Macfarlane, R. J.; Lee, B.; Jones, M. R.; Harris, N.; Schatz, G. C.; Mirkin, C. A. Nanoparticle Superlattice Engineering with DNA. *Science* **2011**, *334*, 204−208.
(6) Liao, C. W.; Lin, Y. S.; Chanda, K.; Song, Y. F.; Huang, M. H. Formation of Diverse Supercrystals from Self-assembly of a Variety of Polyhedral Gold Nanocrystals. *J. Am. Chem. Soc.* **2013**, *135*, 2684−2693.
(7) Young, K. L.; Personick, M. L.; Engel, M.; Damasceno, P. F.; Barnaby, S. N.; Bleher, R.; Li, T.; Glotzer, S. C.; Lee, B.; Mirkin, C. A. A Directional Entropic Force Approach to Assemble Anisotropic Nanoparticles into Superlattices. *Angew. Chem., Int. Ed.* **2013**, *52*, 13980−13984.
(8) Shi, X.; Shen, M.; Möhwald, H. Polyelectrolyte Multilayer Nanoreactors toward the Synthesis of Diverse Nanostructured Materials. *Prog. Polym. Sci.* **2004**, *29*, 987−1019.
(9) Shenhar, R.; Norsten, T. B.; Rotello, V. M. Polymer-Mediated Nanoparticle Assembly: Structural Control and Applications. *Adv. Mater.* **2005**, *17*, 657−669.
(10) Kim, M.; Jeong, G. H.; Lee, K. Y.; Kwon, K.; Han, S. W. Fabrication of nanoporous superstructures through hierarchical self-assembly of nanoparticles. *J. Mater. Chem.* **2008**, *18*, 2208−2212.
(11) Zhang, L.; Song, Y.; Fujita, T.; Zhang, Y.; Chen, M.; Wang, T. H. Large Enhancement of Quantum Dot Fluorescence by Highly Scalable Nanoporous Gold. *Adv. Mater.* **2014**, *26*, 1289−1294.
(12) Kühler, P.; Weber, M.; Lohmüller, T. Plasmonic Nanoantenna Arrays for Surface-Enhanced Raman Spectroscopy of Lipid Molecules Embedded in a Bilayer Membrane. *ACS Appl. Mater. Interfaces* **2014**, *6*, 8947−8952.
(13) Zhang, Q.; Large, N.; Nordlander, P.; Wang, H. Porous Au Nanoparticles with Tunable Plasmon Resonances and Intense Field Enhancements for Single-Particle SERS. *J. Phys. Chem. Lett.* **2014**, *5*, 370−374.
(14) Lee, S. Y.; Kim, S. H.; Kim, M. P.; Jeon, H. C.; Kang, H.; Kim, H. J.; Kim, B. J.; Yang, S. M. Freestanding and Arrayed Nanoporous Microcylinders for Highly Active 3D SERS Substrate. *Chem. Mater.* **2013**, *25*, 2421−2426.
(15) Milner, S. T. Polymer Brushes. *Science* **1991**, *251*, 905−914.
(16) Barbey, R.; Lavanant, L.; Paripovic, D.; Schüwer, N.; Sugnaux, C.; Tugulu, S.; Klok, H. A. Polymer Brushes via Surface-initiated Controlled Radical Polymerization: Synthesis, Characterization, Properties, and Applications. *Chem. Rev.* **2009**, *109* (11), 5437−5527.
(17) Uhlmann, P.; Merlitz, H.; Sommer, J. U.; Stamm, M. Polymer Brushes for Surface Tuning. *Macromol. Rapid Commun.* **2009**, *30*, 732−740.
(18) Fang, M.; Chen, Z.; Wang, S.; Lu, H. The Deposition of Iron and Silver Nanoparticles in Graphene-polyelectrolyte brushes. *Nanotechnology* **2012**, *23*, 085704.
(19) Contreras-Caceres, R.; Dawson, C.; Formanek, P.; Fischer, D.; Simon, F.; Janke, A.; Uhlmann, P.; Stamm, M. Polymers as Templates for Au and Au@Ag Bimetallic Nanorods: UV-Vis and Surface Enhanced Raman Spectroscopy. *Chem. Mater.* **2013**, *25*, 158−169.
(20) Gupta, S.; Agrawal, M.; Conrad, M.; Hutter, N. A.; Olk, P.; Simon, F.; Eng, L. M.; Stamm, M.; Jordan, R. Poly(2-(dimethylamino)ethyl methacrylate) Brushes with Incorporated Nanoparticles as a SERS Active Sensing Layer. *Adv. Funct. Mater.* **2010**, *20*, 1756−1761.
(21) Steenackers, M.; Lud, S. Q.; Niedermeier, M.; Bruno, P.; Gruen, D. M.; Feulner, P.; Stutzmann, M.; Garrido, J. A.; Jordan, R. Structured Polymer Grafts on Diamond. *J. Am. Chem. Soc.* **2007**, *129*, 15655−15661.
(22) Tran, Y.; Auroy, P. Synthesis of Poly(styrene sulfonate) Brushes. *J. Am. Chem. Soc.* **2001**, *123*, 3644−3654.
(23) Wang, H. L.; Brown, H. R. Self-Initiated Photopolymerization and Photografting of Acrylic Monomers. *Macromol. Rapid Commun.* **2004**, *25*, 1095−1099.
(24) Kim, J.; Seidler, P.; Wan, L. S.; Fill, C. Formation, Structure, and Reactivity of Amino-terminated Organic Films on Silicon Substrates. *J. Colloid Interface Sci.* **2009**, *329*, 114−119.

(25) Dutta, S.; Ray, C.; Sarkar, S.; Pradhan, M.; Negishi, Y.; Pal, T. Silver Nanoparticle Decorated Reduced Graphene Oxide (rGO) Nanosheet: A Platform for SERS Based Low-Level Detection of Uranyl Ion. *ACS Appl. Mater. Interfaces* **2013**, *5*, 8724−8732.
(26) Ciszek, J. W.; Huang, L.; Tsonchev, S.; Wang, Y. H.; Shull, K. R.; Ratner, M. A.; Schatz, G. C.; Mirkin, C. A. Assembly of Nanorods into Designer Superstructures: the Role of Templating, Capillary Forces, Adhesion, and Polymer Hydration. *ACS Nano* **2010**, *4*, 259−266.
(27) Choi, J. J.; Bian, K.; Baumgardner, W. J.; Smilgies, D. M.; Hanrath, T. Interface-Induced Nucleation, Orientational Alignment and Symmetry Transformations in Nanocube Superlattices. *Nano Lett.* **2012**, *12*, 4791−4198.
(28) Liu, Z.; Pappacena, K.; Cerise, J.; Kim, J.; Durning, C. J.; O'Shaughnessy, B.; Levicky, R. Organization of Nanoparticles on Soft Polymer Surfaces. *Nano Lett.* **2002**, *2*, 219−224.
(29) Ciebien, J. F.; Clay, R. T.; Sohn, B. H.; Cohen, R. E. Brief Review of Metal Nanoclusters in Block Copolymer Films. *New J. Chem.* **1998**, *22*, 685−691.
(30) Kim, J. U.; O'Shaughnessy, B. Morphology Selection of Nanoparticle Dispersions by Polymer Media. *Phys. Rev. Lett.* **2002**, *89*, 238301.
(31) Orski, S. V.; Fries, K. H.; Sontag, S. K.; Locklin, J. Fabrication of Nanostructures Using Polymer Brushes. *J. Mater. Chem.* **2011**, *21*, 14135−14149.
(32) Cölfen, H.; Antonietti, M. Mesocrystals: Inorganic Superstructures Made by Highly Parallel Crystallization and Controlled Alignment. *Angew. Chem., Int. Ed.* **2005**, *44*, 5576−5591.
(33) Sun, X.; Wei, W. Electrostatic-Assembly-Driven Formation of Micrometer-Scale Supramolecular Sheets of (3-Aminopropyl)-triethoxysilane(APTES)-$HAuCl_4$ and Their Subsequent Transformation into Stable APTES Bilayer-Capped Gold Nanoparticles through a Thermal Process. *Langmuir* **2010**, *26*, 6133−6135.
(34) Zhang, D.; Jin, Y.; Cheng, J.; Jiang, Y.; He, L.; Zhang, L. Self-Assembly of Nanorod/Nanoparticle Mixtures in Polymer Brushes. *J. Poly. Sci., Part B: Poly. Phys.* **2014**, *52*, 299−309.
(35) Sun, X.; Du, Y.; Zhang, L.; Dong, S.; Wang, E. Luminescent Supramolecular Microstructures Containing $Ru(bpy)_3^{2+}$: Solution-Based Self-Assembly Preparation and Solid-State Electrochemiluminescence Detection Application. *Anal. Chem.* **2007**, *79*, 2588−2592.
(36) Fang, J.; Du, S.; Lebedkin, S.; Li, Z.; Kruk, R.; Kappes, M.; Hahn, H. Gold Mesostructures with Tailored Surface Topography and Their Self-Assembly Arrays for Surface-Enhanced Raman Spectroscopy. *Nano Lett.* **2010**, *10*, 5006−5013.
(37) Liu, Z.; Yang, Z.; Peng, B.; Cao, C.; Zhang, C.; You, H.; Xiong, Q.; Li, Z.; Fang, J. Highly Sensitive, Uniform, and Reproducible Surface-Enhanced Raman Spectroscopy from Hollow Au-Ag Alloy Nanourchins. *Adv. Mater.* **2014**, *26*, 2431−2439.
(38) Li, X.; Choy, W. C. H.; Ren, X.; Zhang, D.; Lu, H. Highly Intensified Surface Enhanced Raman Scattering by Using Monolayer Graphene as the Nanospacer of Metal Film-Metal Nanoparticle Coupling System. *Adv. Funct. Mater.* **2014**, *24*, 3114−3122.
(39) Michaels, A. M.; Nirmal, M.; Brus, L. E. Surface Enhanced Raman Spectroscopy of Individual Rhodamine 6G Molecules on Large Ag Nanocrystals. *J. Am. Chem. Soc.* **1999**, *121*, 9932−9939.
(40) Fan, Z.; Kanchanapally, R.; Chandra Ray, P. Hybrid Graphene Oxide Based Ultrasensitive SERS Probe for Label-Free Biosensing. *J. Phys. Chem. Lett.* **2013**, *4*, 3813−3818.
(41) Le Ru, E. C.; Blackie, E.; Meyer, M.; Etchegoin, P. G. Surface Enhanced Raman Scattering Enhancement Factors: A Comprehensive Study. *J. Phys. Chem. C* **2007**, *111*, 13794−13803.
(42) Oh, Y. J.; Jeong, K. H. Glass Nanopillar Arrays with Nanogap-Rich Silver Nanoislands for Highly Intense Surface Enhanced Raman Scattering. *Adv. Mater.* **2012**, *24*, 2234−2237.